Magnetic Resonance in Medicine 50:1061–1068 (2003)

Accuracy and Reproducibility in Phase Contrast Imaging Using SENSE

Per Thunberg,[1–3]* Matts Karlsson,[2] and Lars Wigström[2,3]

The purpose of this study was to evaluate the accuracy and reproducibility of phase contrast imaging using the sensitivity encoding (SENSE) method at different reduction factors. Analytical expressions were derived that state how reproducibility is influenced for velocity and flow measurements. Computer simulations, and in vitro and in vivo studies were performed in order to validate these expressions and to assess how accuracy is affected when different reduction factors are applied. It was shown that reproducibility depends on the reduction and geometry factors. Since the geometry factor varies spatially, so does the reproducibility for phase contrast imaging. In areas with high geometry factors, the standard deviation (SD) may become so large that aliasing occurs. The accuracy of phase contrast imaging is not influenced directly when SENSE is used, but may be indirectly influenced due to high SDs of the measured phase that may subsequently cause aliasing. The current results show that it is possible to achieve accurate flow measurements even at high reduction factors. By taking the geometry factor into account, it may be possible to find areas where phase contrast imaging is accurate even at high reduction factors. Magn Reson Med 50:1061–1068, 2003. © 2003 Wiley-Liss, Inc.

Key words: phase contrast imaging; flow quantification; SENSE; parallel MRI; reproducibility

The development of parallel acquisition strategies in magnetic resonance imaging (MRI) has created a potential for dramatic decreases in scan times. Several approaches for reconstructing images from individual coil elements have been proposed, based on combining the signal from individual coil elements in either the Fourier (1,2) or spatial (3,4) domain. The sensitivity encoding (SENSE) method has been shown to be a robust approach to image reconstruction (5), and has been implemented in many different pulse sequences, including non-Cartesian sampling patterns (6). With SENSE, the reduction in scan time can be selected depending on the number of coils used for parallel data acquisition. The SENSE method can also be used to suppress pulsation artifacts, with the same scan times as used in conventional acquisition methods (7).

Phase contrast imaging is an established method that allows the velocities of moving spins to be measured (8–12), and is widely used to quantify blood flow (13) and cardiac motion (14,15). The accuracy and reproducibility of phase contrast imaging have been thoroughly investigated, and a number of factors that influence the measured phase values have been identified (16). With compensation for these known artifacts, the phase contrast method has been shown to be very accurate (12,17,18). The acquisition time of phase contrast imaging can be relatively long, however, especially when all three velocity components are measured. Significant reductions in scan time would be highly useful, and may be achieved by using SENSE in combination with phase contrast imaging.

The aim of this study was to determine what impact the use of SENSE at different reduction factors would have on the accuracy and reproducibility of phase contrast imaging. Computer simulations, and in vitro and in vivo studies were used to validate analytical expressions derived for the prediction of the standard deviations (SDs) of the induced phase shifts.

METHODS

The basic principle in Cartesian SENSE is to acquire images from different coils with a field of view (FOV) that has been reduced by a reduction factor R. A reduction of the FOV implies that complex voxel signals, which in the full-FOV image are separated by a distance equal to the reduced FOV, are superimposed in the reconstructed images. With the use of a priori knowledge of each coil's sensitivity, the SENSE method separates these superimposed signals and places them at their correct positions in one full-FOV image, free from wraparound artifacts. By employing the complex valued coil sensitivities in the SENSE reconstruction, magnitude as well as valid phase images can be calculated. The accuracy of the coils' sensitivity maps is crucial for accurate SENSE reconstruction (3).

THEORY

The SD for the induced phase shift ϕ in a reconstructed image using the two-point phase contrast acquisition method can be expressed as (19)

$$\sigma_\phi = \frac{\sqrt{2}}{\mathrm{SNR}} \qquad [1]$$

where SNR is the signal-to-noise ratio in one magnitude image, and $\sqrt{2}$ is a gain due to the subtraction of the two acquired phases which are obtained with opposite first gradient moments. Equation [1] does not depend on ϕ and is valid in pixels where the signal is greater than twice the SD of the background noise. The induced phase shift can be converted to velocity by multiplication with the constant Venc/π. The velocity encoding (Venc) corresponds to

[1]Department of Biomedical Engineering, Örebro University Hospital, Örebro, Sweden.

[2]Department of Biomedical Engineering, Linköping University, Linköping, Sweden.

[3]Department of Medicine and Care, Division of Clinical Physiology, Linköping University, Linköping, Sweden.

*Correspondence to: Per Thunberg, M.Sc., Department of Biomedical Engineering, Örebro University Hospital, S-70185 Örebro, Sweden. E-mail: per.thunberg@orebroll.se

Received 24 February 2003; revised 28 May 2003; accepted 22 July 2003.

DOI 10.1002/mrm.10634

Published online in Wiley InterScience (www.interscience.wiley.com).

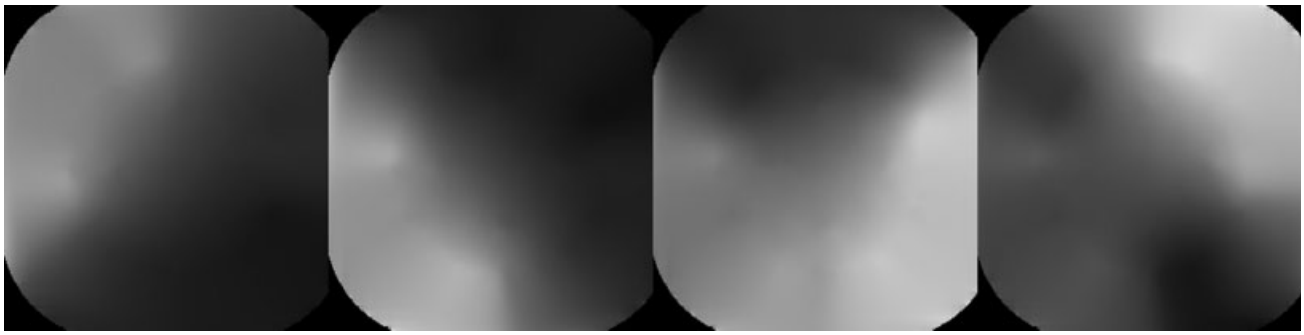

FIG. 1. Magnitude images of the sensitivity maps used in the simulation. These sensitivity maps were calculated based on actual image data acquired using a four-element coil array.

the velocity that induces a phase shift velocity encoding (venc) of π radians (11).

When the SENSE technique is used with a reduction factor R, the SNR in one pixel, indexed ρ, is changed according to

$$\mathrm{SNR}_\rho^R = \frac{\mathrm{SNR}_\rho^{\mathrm{full}}}{g_\rho \sqrt{R}} \quad [2]$$

where g is the geometry factor defined by Pruessmann et al. (3). The term $\mathrm{SNR}^{\mathrm{full}}$ corresponds to the SNR in a reconstructed image with SENSE having R set to one. When Eq. [1] is combined with Eq. [2], the SDs for the induced phase shift in a SENSE acquisition is given by

$$\sigma_{\phi,\rho}^R = \frac{\sqrt{2} g_\rho \sqrt{R}}{\mathrm{SNR}_\rho^{\mathrm{full}}} \quad [3]$$

The flow rate through a region of interest (ROI) can be calculated by multiplying the mean phase value measured within an ROI with Venc/π and the area of the ROI, A_{ROI}. The SD for the flow at a certain reduction factor is then given by

$$\sigma_f^R = \frac{A_{\mathrm{ROI}} Venc \sqrt{2}}{N\pi} \sqrt{\sum_{\rho \in \mathrm{ROI}} \left(\frac{g_\rho \sqrt{R}}{\mathrm{SNR}_\rho^{\mathrm{full}}} \right)^2} \quad [4]$$

where N is the number of voxels within the ROI. Assuming constant SNR in the full-FOV magnitude image within the ROI, the SD for flow measurements at a certain reduction factor can be expressed as

$$\sigma_f^R = \frac{\sigma_f^{R=1}}{\sqrt{N}} \sqrt{\sum_{\rho \in \mathrm{ROI}} (g_\rho \sqrt{R})^2} \quad [5]$$

where $\sigma_f^{R=1}$ is the SD for flow measurements at $R = 1$.

Simulations

Computer simulations were performed to define the impact of SENSE at different reduction factors on the accuracy and reproducibility of phase contrast imaging. Actual coil sensitivity maps were obtained by imaging a static phantom using a 1.5T Signa Horizon EchoSpeed scanner (General Electric Medical Systems, Milwaukee, WI) with the body coil and a four-element, phased-array torso coil. The calculation of the coil sensitivities for each element in the phased-array coil included pixel-wise complex division, smoothing, and extrapolation.

The measured complex coil sensitivity maps (Fig. 1) were used in a simulation designed to validate the expressions for reproducibility. A theoretical phantom was designed with a constant magnitude of one and a phase of zero. Subsequent addition of a phase ϕ to all four coil images should result in a SENSE reconstructed image with a constant signal magnitude of one and a phase equal to ϕ.

A set of phantom images (2400 phases $\times$ two echoes $\times$ four coils) was created. Each image had a matrix size of 256×256. The measurement associated with the first echo was given a phase value of 0.5ϕ, and the second echo was assigned a phase value of -0.5ϕ. Thus, the net induced phase shift obtained after subtraction was ϕ. Four different phase values were used: $\phi = 0$, $\pi/4$, $\pi/2$ and $3\pi/4$. Gaussian noise with a zero mean was added independently to the real and imaginary parts of each coil image before reconstruction. The SNR in an image reconstructed from the four individual coil images with $R = 1$ was 40 dB. Each image was multiplied by the corresponding coil sensitivity map, folded according to $R = 2$, 3, and 4, and then reconstructed using the SENSE method. The phase images obtained from the two echoes were subtracted in order to get the final phase image. The total number of reconstructed images was 2400 for each simulated phase value and reduction factor.

In Vitro Study

The in vitro study was performed using a stationary phantom. Phase contrast measurements were performed using a prospectively gated 2D pulse sequence. A series of 30 images were reconstructed. The following parameters were used: flip angle = 20°, FOV = 300 mm, matrix = 256×256, TR/TE = 8.3/3.1 ms, Venc = 1.5 m/s, one view per segment, and slice thickness = 10 mm. As in the computer simulation, each acquired image was then folded corresponding to $R = 2$, 3, and 4 by using only every second, third, and fourth k-space line of the acquired data. Sensitivity reconstruction was used to reconstruct the folded images to full FOV.

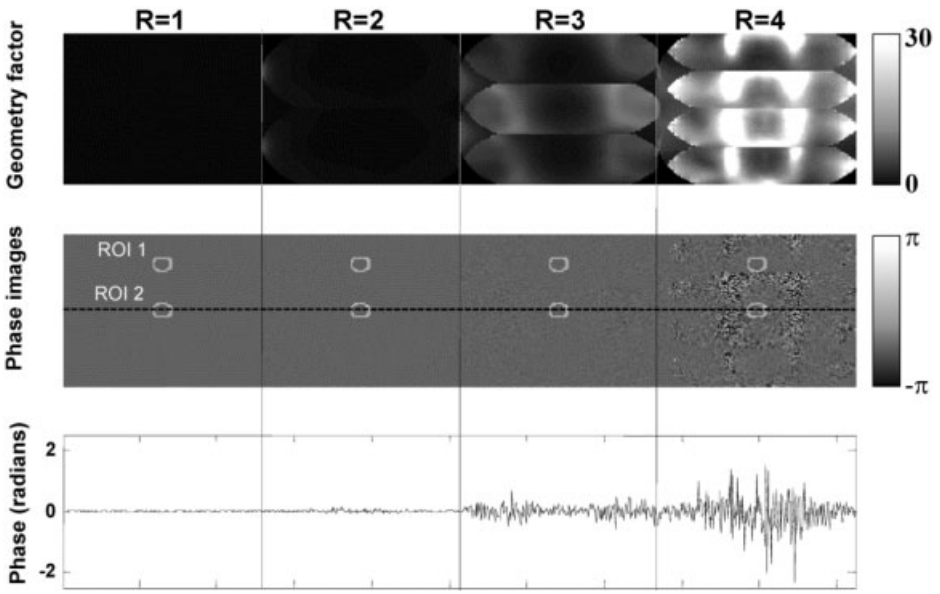

FIG. 2. Geometry factors (upper panel) and phase images (middle panel) for different reduction factors (R = 1, 2, 3, 4) The two ROIs (ROI 1 and ROI 2) were used for statistical analysis. In the lower panel the phase values are plotted along the dashed line seen in the middle figure. The phase images shown represent simulations for $\phi = 0$.

The reference images required for determination of the sensitivity maps were obtained using the body coil and a four-element, phased-array torso coil. All reference images were obtained using a gradient-echo pulse sequence with the following parameters applied: flip angle = 20°, FOV = 300 mm, matrix = 256 × 256, TR/TE = 8.3/3.2 ms, and slice thickness = 10 mm.

In Vivo Study

The blood flow in the ascending and descending aortas was measured in a healthy volunteer using a prospective ECG-triggered phase contrast pulse sequence with the following parameters: flip angle = 20°, TR/TE = 7.8/2.9, FOV = 300 × 400 mm, matrix = 96 × 256, slice thickness = 10 mm, four views per segment, and Venc = 1.5 m/s. The total acquisition time was 22 s, which allowed breath-holding during the scan. The total number of reconstructed phases was 19. All images were folded corresponding to R = 2, 3, and 4, and then reconstructed to full-FOV images using SENSE. The images required for calculation of the sensitivity maps were obtained during breath-hold using a gradient-echo pulse sequence with the same parameters as for the phase contrast measurement, except that TR/TE = 7/3.1 ms.

RESULTS

Simulations

The phase images obtained using four different reduction factors are shown in Fig. 2. The two ROIs shown were used to analyze accuracy and reproducibility.

The simulated mean values and SDs for the phase values in the center voxel for both ROIs are shown for different reduction factors in Table 1. According to Eq. [3], the SD for the induced phase shift is increased by a factor $\sqrt{R}g$ compared to the SD obtained with $R = 1$. For a comparison of the stimulated and thetheoretically calculated SDs, the phase SD for $R = 1$ was multiplied by $\sqrt{R}$ and the geometry factor value for the actual position.

The simulated phase values agreed well with the true values, except for $R = 4$ in ROI 2. This is illustrated in Fig.

Table 1
Mean Phase Values and Standard Deviations for the Center Voxel in Each ROI Through the Sequence of 2400 Simulated Images for Different Reduction Factors

True phase shift (radians)	Simulated phase shift (radians)							
	Center pixel in ROI 1				Center pixel in ROI 2			
	R = 1	R = 2	R = 3	R = 4	R = 1	R = 2	R = 3	R = 4
$\phi = 0$	0.00 ± 0.02	0.00 ± 0.02	0.00 ± 0.04	0.01 ± 0.15	0.00 ± 0.02	0.00 ± 0.04	0.00 ± 0.08	0.01 ± 0.57
$\phi = \pi/4$ (≈ 0.79)	0.79 ± 0.02	0.79 ± 0.02	0.78 ± 0.04	0.79 ± 0.16	0.79 ± 0.02	0.79 ± 0.04	0.79 ± 0.08	0.76 ± 0.56
$\phi = \pi/2$ (≈ 1.57)	1.57 ± 0.02	1.57 ± 0.02	1.57 ± 0.04	1.57 ± 0.15	1.57 ± 0.02	1.57 ± 0.04	1.57 ± 0.08	1.56 ± 0.63
$\phi = 3\pi/4$ (≈ 2.36)	2.36 ± 0.02	2.36 ± 0.02	2.36 ± 0.04	2.35 ± 0.16	2.36 ± 0.02	2.36 ± 0.04	2.36 ± 0.08	1.93 ± 1.37
Theoretically calculated SD	0.02	0.02	0.04	0.16	0.02	0.04	0.08	0.52

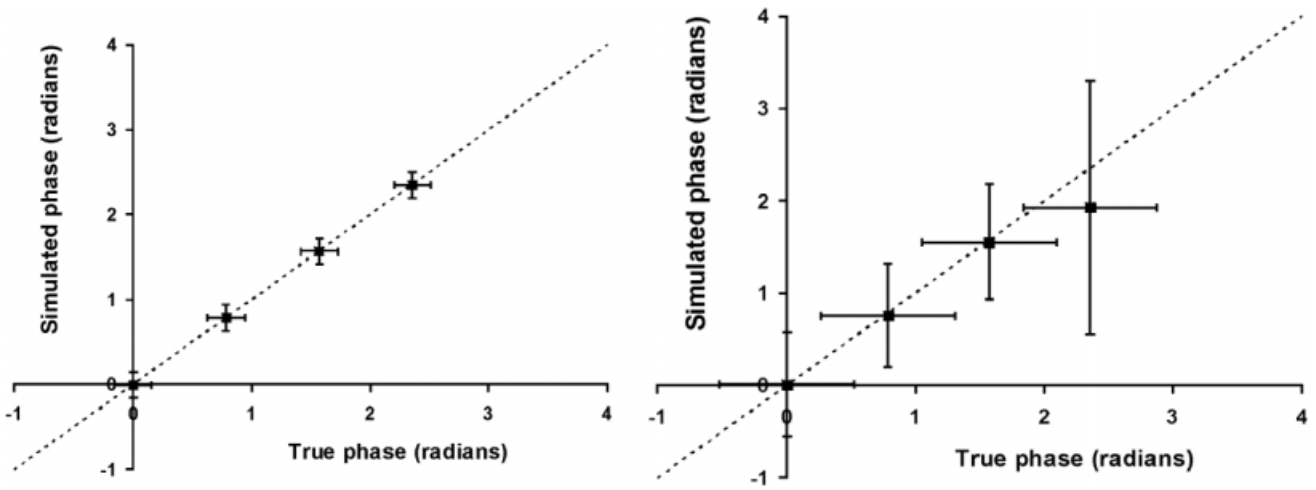

FIG. 3. True and measured phases in the center voxels of ROI 1 (left panel) and ROI 2 (right panel) at reduction factor 4. The theoretically calculated SDs are shown as horizontal bars, while the SDs for the measured phases are shown as vertical bars. The dotted lines represent the line of identity.

3, in which the true and simulated mean phase values are shown with the SDs for the center voxels in ROIs 1 and 2 at reduction factor 4. In the left panel of Fig. 3, the agreement between the simulated and expected SDs, and between the simulated and true phase values are excellent. However, in the right panel of Fig. 3, the difference between the mean simulated phase values and SDs and the theoretical values and SDs is noticeable.

An alternative perspective on the data is shown in Fig. 4, in which histograms for all simulated phase values at reduction factor 4 are shown for the center voxels in ROI 2. Up to $\phi = \pi/2$ the histograms have a Gaussian distribution, with an SD predicted by Eq. [3]. However, at $\phi = 3\pi/4$ some phase measurements exceed π, and consequently are aliased and appear as negative phase values.

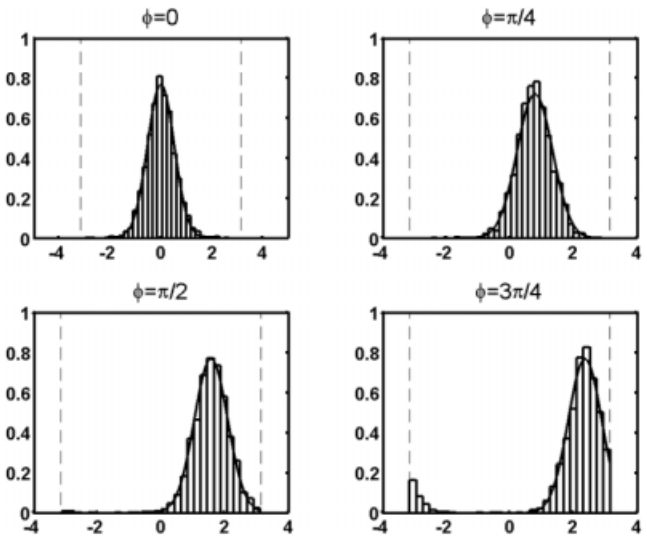

FIG. 4. Normalized histograms for all phase measurements for the center voxel of ROI 2 at reduction factor 4. The solid curves correspond to a Gaussian function with mean values equivalent to the true phase values and theoretically calculated SDs (see Table 1).

The measured mean and SDs for the mean phase values in each ROI are shown in Table 2. Excellent agreements between simulated and expected values are obtained, except for ROI 2 at reduction factor 4.

The histograms in Fig. 5 show the distribution of the mean phase values for all voxels within ROI 2 at $R = 4$. A good agreement is obtained between the histogram and the expected Gaussian curve when the true phase for all voxels is zero (Fig. 5a). In Fig. 5b–d it becomes apparent that the histograms have a lower mean and a broader distribution than expected.

In Vitro Study

Reconstructed magnitude and phase images of the in vitro phantom are shown in Fig. 6 for the reduction factors $R = 1, 2, 3$, and 4. Figure 7 shows the normalized histograms of the phase distributions of all voxels for the 30 different images within each ROI in Fig. 6. The solid line corresponds to the expected distribution, with a mean of zero and SD calculated from Eq. [3]. Theoretical SDs were calculated from the mean g-value in each ROI together with $\sqrt{R}$.

In Vivo Study

Reconstructed magnitude and phase images from the fifth time frame in the cardiac cycle (systole) are shown Fig. 8. Flow curves measured in the ascending and descending aortas are shown in Fig. 9. The flow curves obtained for different reduction factors have similar shapes when the flow is measured in the ascending aorta, but in the descending aorta the systolic flow measured for $R = 4$ is lower than the other three.

DISCUSSION

The use of SENSE offers potentially significant reductions in scan time for phase contrast imaging, which is the basis for many cardiovascular applications. It is therefore im-

Table 2
The Mean and Standard Deviations of the Mean Phase in Each ROI for Different Reduction Factors*

True mean phase within ROI (radians)	Simulated mean phase within ROI (radians)							
	ROI 1				ROI 2			
	R = 1	R = 2	R = 3	R = 4	R = 1	R = 2	R = 3	R = 4
$\phi = 0$	0 ± 0.001	0 ± 0.001	0 ± 0.003	0 ± 0.009	0 ± 0.001	0 ± 0.002	0 ± 0.005	0 ± 0.04
$\phi = \pi/4$ (≈ 0.785)	0.785 ± 0.001	0.785 ± 0.001	0.785 ± 0.003	0.785 ± 0.009	0.785 ± 0.001	0.785 ± 0.001	0.786 ± 0.002	0.77 ± 0.04
$\phi = \pi/2$ (≈ 1.571)	1.571 ± 0.001	1.571 ± 0.001	1.571 ± 0.002	1.571 ± 0.009	1.571 ± 0.001	1.571 ± 0.002	1.571 ± 0.005	1.48 ± 0.04
$\phi = 3\pi/4$ (≈ 2.356)	2.356 ± 0.001	2.356 ± 0.001	2.356 ± 0.003	2.356 ± 0.009	2.356 ± 0.001	2.356 ± 0.001	2.356 ± 0.002	1.71 ± 0.09
Theoretically calculated SD	0.001	0.001	0.003	0.009	0.001	0.002	0.005	0.03

*The mean phase, in each image, was obtained by averaging all pixel values within the ROI.

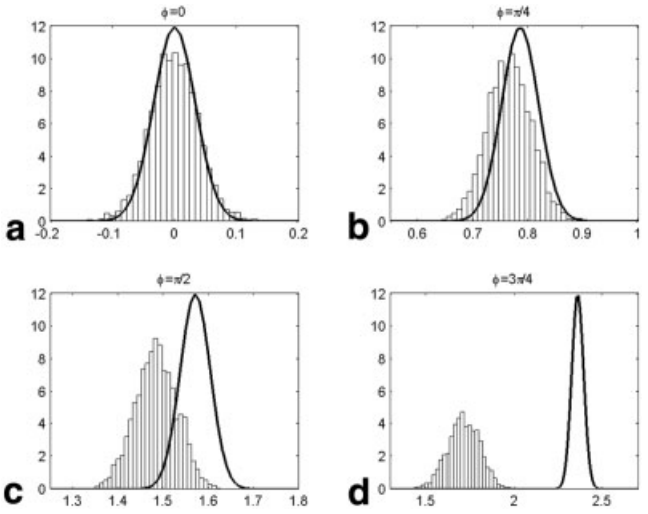

FIG. 5. Normalized histograms for the mean phase value within ROI 2 through all 2400 phases at reduction factor 4. The solid curves correspond to Gaussian functions with mean values equal to the true mean values and SDs equal to the theoretically calculated. **a–d:** Four different phase values ($\phi = 0$, $\pi/4$, $\pi/2$, and $3\pi/4$) were simulated.

portant to determine whether the accuracy and reproducibility of phase contrast imaging is affected by SENSE.

In this study there was excellent agreement between the simulated and true phase values and SDs. The data suggest that the change in reproducibility in phase contrast imaging using SENSE compared to conventional full-FOV imaging can be accurately predicted by the use of Eqs. [3]–[5].

It was also demonstrated that the SDs of the induced phase shifts vary spatially when SENSE is used. This is a consequence of the geometry factor, which depends on the number of coils used and the actual coil setup. Figure 2 describes the spatial variation of the geometry factor, and how the noise in the phase images varies accordingly.

The validity of the derived expressions for reproducibility holds despite prominent noise in the reconstructed images. However, a discrepancy between the simulated and true phase values, as well as the SDs, is noticeable at the location of the center voxel in ROI 2 for reduction factor 4. This difference is illustrated in the right panel of Fig. 3, where the simulated phase value of $\phi = 3\pi/4$ is significantly lower than the true phase value, and the simulated SD is larger than expected. The explanation for this is found in the histograms in Fig. 4. The distribution of the phase values stays the same in the four subfigures, while the mean phase values change. Aliasing occurs as the mean phase value comes closer to π. A higher SD and mean phase value compared to π implies aliasing and, accordingly, that it is no longer possible to predict the SD using only the geometry factor and *R*. Even though the *g*-values increase at higher reduction factors, in some regions it remains possible to predict the SDs at high reduction factors, as shown in the left panel in Fig. 3.

The flow through an ROI is calculated as the mean phase value within the ROI times the area of the ROI. The effect of SENSE on the reproducibility of flow measurements can be reliably predicted by Eq. [4], as shown by the excellent

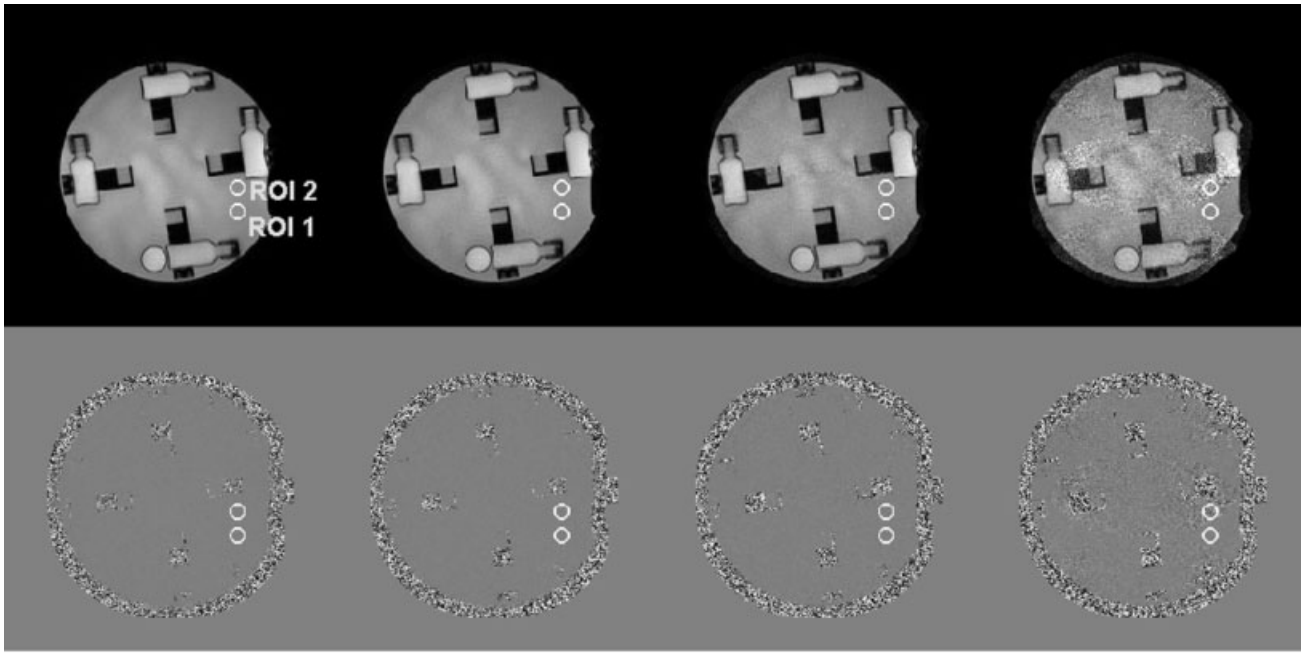

FIG. 6. In the upper panel, reconstructed magnitude images of the stationary phantom are shown for $R = 1, 2, 3$, and 4. In the row below, the corresponding phase images are displayed. ROI 1 and ROI 2 were used for further statistical analysis.

agreement between the simulated mean phase values and the true mean phase values (Table 2). However, at reduction factor 4 a difference becomes apparent in ROI 2 as the true mean phase increases. The illustration in Fig. 5 between simulated and expected distributions indicates

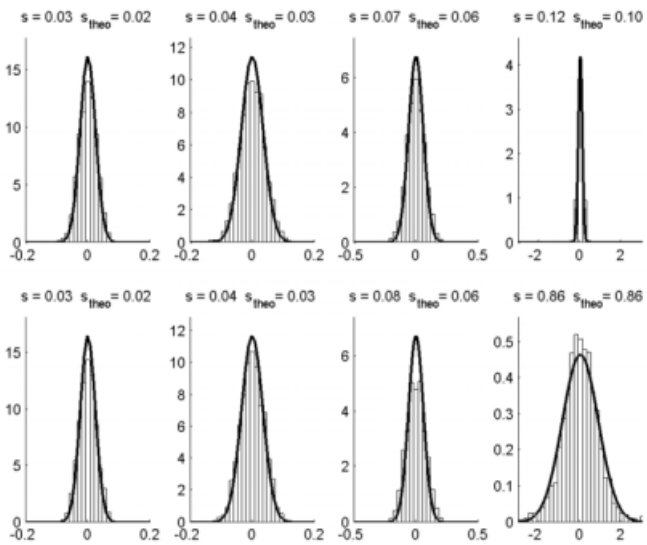

FIG. 7. Normalized histogram distributions for measured phase values within ROI 1 and ROI 2 across the 30 acquired images. The upper and lower rows of figures correspond to ROI 1 and ROI 2, respectively. The columns correspond to $R = 1, 2, 3$, and 4, respectively. The Gaussian functions were calculated with a mean of zero and a SD according to Eq. [3]. Measured and calculated SDs are plotted above each figure. Note that the scale along the x-axis changes for the different reduction factors (s = measured SD, s_{theo} = theoretically expected SD).

a good agreement between simulated and true values for $\phi = 0$. The agreement is gradually degraded as the true mean phase value increases. At $\phi = 3\pi/4$ the simulated mean phase value is 27% lower than the true value, and the SD has increased compared to the expected SD. These discrepancies are explained by the aliasing that can be observed in some voxels (Fig. 4). The aliasing results in a lower mean phase value than expected. As a result, under such circumstances Eq. [4] is no longer able to predict the SDs of flow measurements.

The magnitude and phase images of the in vitro phantom in Fig. 6 clearly illustrate how noise varies spatially in the image due to the geometry factor. ROI 1 was chosen to encompass a region less affected by noise compared to ROI 2. As expected, the SDs of the measured phase shifts within each ROI increased with the reduction factor. Also, the geometrical dependency of the reproducibility becomes clear when one compares the curves for the two ROIs at the same reduction factor. This effect is most evident in a comparison of the two histograms for reduction factor 4. A good agreement between calculated and measured SDs was achieved.

In the in vivo study, blood flow was measured through-plane in both the ascending and descending aortas (Fig. 8). The magnitude images demonstrate how the noise becomes significant at reduction factors 3 and 4, especially in the central parts of the image. In the ascending aorta the flow curves are nearly identical at all four reduction factors (Fig. 9). In contrast, the measured flow in the descending aorta is reduced for a number of time frames for $R = 4$. This nonphysiological flow curve can be explained by the aliasing that occurs in some voxels, which in turn depends upon the geometry factor values and how close the measured velocities are to Venc. In this case the mean

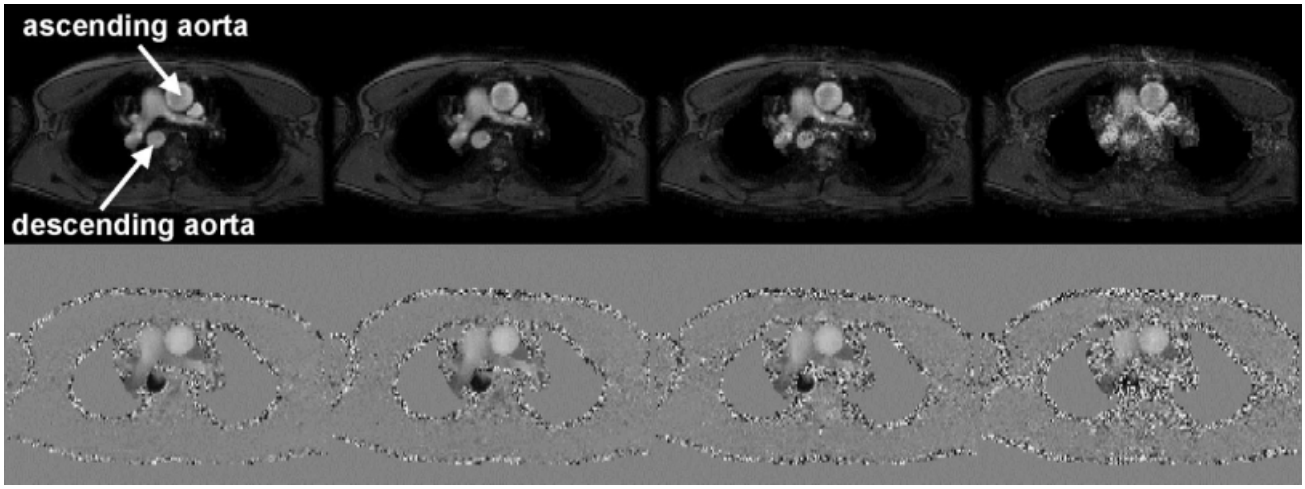

FIG. 8. Reconstructed magnitude (above) and phase (below) images for the in vivo study using $R = 1$, 2, 3, and 4.

geometry factor for $R = 4$ in the ascending aorta was 0.6 ± 0.1, vs. 4.3 ± 0.4 in the descending aorta. The mean velocity in the ascending aorta was 0.6 ± 0.1 m/s, and 1.0 ± 0.3 m/s in the descending aorta. The higher velocities and geometry factors resulted in aliasing in some voxels in the descending aorta, but not in the ascending aorta for $R = 4$. This is in keeping with the results obtained in both the simulations and the in vitro studies.

The accuracy of phase contrast imaging may be indirectly influenced when the SDs of the induced phase shifts become so large that aliasing occurs. In that case, an increase of the Venc would improve the accuracy, since the difference between the induced phase shift and the threshold for aliasing would increase. However, an improved accuracy obtained by such action would proportionally increase the SD of the induced phase shift. An adjustment between accuracy and reproducibility is therefore necessary. Nevertheless, it is possible to obtain accurate phase contrast measurements even at high reduction factors if the ROI is located in an area of low *g*-values.

Accuracy in conventional phase contrast imaging is hampered by phase offsets that do not originate from the motion of the spins—for example, eddy currents (12) and Maxwell terms (17). These artifacts will appear similar in SENSE-reconstructed images, but with the characteristic varying noise enhancement that follows the SENSE method (3).

The SNR and geometry factor values strongly influence the reproducibility of SENSE phase contrast imaging. Optimization and control of SENSE phase contrast imaging therefore requires understanding of the parameters that affect the SNR and the geometry factor. The development

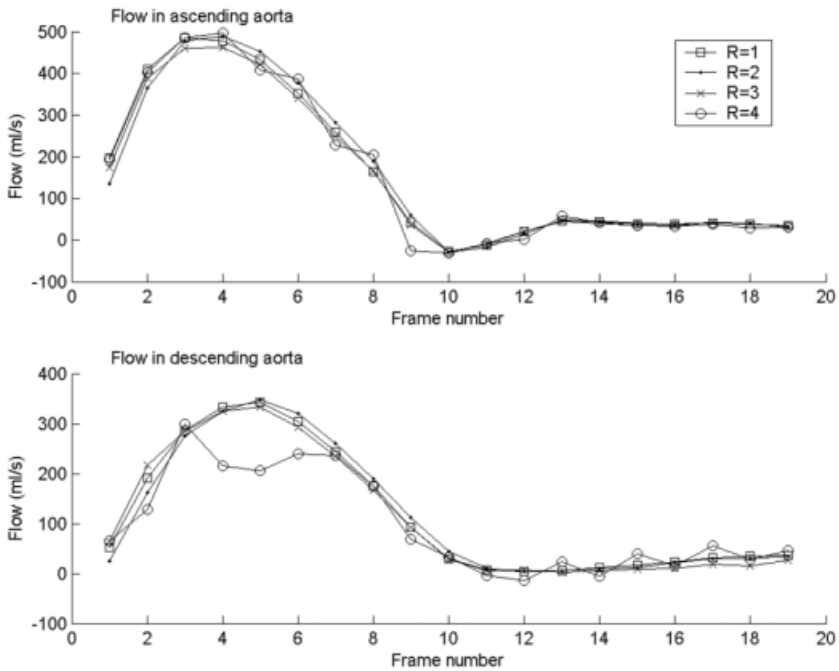

FIG. 9. Blood flow in the ascending and descending aortas at different reduction factors.

of coils dedicated for parallel MRI requires that the SNR be optimized for the number of coils being used (20,21). Coil coupling between the different coils has been discussed as a potential problem that could decrease the SNR in the reconstructed images. However, recent studies have shown that this effect has a very limited impact on the SNR (22,23). One very efficient way to improve the SNR is to exclude voxels in the reconstruction that are empty in the sensitivity maps and thus do not contribute any signal to the superimposed voxels (24).

The ability to predict reproducibility when using SENSE at a given reduction factor may become a useful tool for preparing flow measurements. The necessary information for such prediction is given by the geometry factor, which is calculated from the actual coil sensitivities. Since the coil sensitivities are determined at an early stage in an examination involving SENSE, a priori information regarding how the SD in a specific region will be influenced at a certain reduction factor could be obtained. This would enable one to, for example, modify coil placement to improve image quality.

In conclusion, the impact of SENSE on the accuracy and reproducibility of phase contrast imaging is predictable and can be taken into account. It is possible to obtain accurate velocity measurements even at high reduction factors, depending on where the ROI is located.

ACKNOWLEDGMENTS

The authors thank Dr. Ann Bolger for constructive comments on this work.

REFERENCES

1. Sodickson DK, Manning WJ. Simultaneous acquisition of spatial harmonics (SMASH): fast imaging with radiofrequency coil arrays. Magn Reson Med 1997;38:591–603.
2. Griswold MA, Jakob PM, Heidemann RM, Nittka M, Jellus V, Wang J, Kiefer B, Haase A. Generalized autocalibrating partially parallel acquisitions (GRAPPA). Magn Reson Med 2002;47:1202–1210.
3. Pruessmann KP, Weiger M, Scheidegger MB, Boesiger P. SENSE: sensitivity encoding for fast MRI. Magn Reson Med 1999;42:952–962.
4. Griswold MA, Jakob PM, Nittka M, Goldfarb JW, Haase A. Partially parallel imaging with localized sensitivities (PILS). Magn Reson Med 2000;44:602–609.
5. Madore B, Pelc NJ. SMASH and SENSE: experimental and numerical comparisons. Magn Reson Med 2001;45:1103–1111.
6. Pruessmann KP, Weiger M, Bornert P, Boesiger P. Advances in sensitivity encoding with arbitrary k-space trajectories. Magn Reson Med 2001;46:638–651.
7. Kellman P, McVeigh ER. Ghost artifact cancellation using phased array processing. Magn Reson Med 2001;46:335–343.
8. Moran PR. A flow velocity zeugmatographic interlace for NMR imaging in humans. Magn Reson Imaging 1982;1:197–203.
9. Nayler GL, Firmin DN, Longmore DB. Blood flow imaging by cine magnetic resonance. J Comput Assist Tomogr 1986;10:715–722.
10. Dumoulin CL, Souza SP, Feng H. Multiecho magnetic resonance angiography. Magn Reson Med 1987;5:47–57.
11. Pelc NJ, Herfkens RJ, Shimakawa A, Enzmann DR. Phase contrast cine magnetic resonance imaging. Magn Reson Q 1991;7:229–254.
12. Pelc NJ, Sommer FG, Li KC, Brosnan TJ, Herfkens RJ, Enzmann DR. Quantitative magnetic resonance flow imaging. Magn Reson Q 1994; 10:125–147.
13. Ståhlberg F, Sondergaard L, Thomsen C. MR flow quantification with cardiovascular applications: a short overview. Acta Paediatr Suppl 1995;410:49–56.
14. Wedeen VJ. Magnetic resonance imaging of myocardial kinematics. Technique to detect, localize, and quantify the strain rates of the active human myocardium. Magn Reson Med 1992;27:52–67.
15. Arai AE, Gaither 3rd CC, Epstein FH, Balaban RS, Wolff SD. Myocardial velocity gradient imaging by phase contrast MRI with application to regional function in myocardial ischemia. Magn Reson Med 1999;42: 98–109.
16. Buonocore MH, Bogren H. Factors influencing the accuracy and precision of velocity-encoded phase imaging. Magn Reson Med 1992;26: 141–154.
17. Bernstein MA, Zhou XJ, Polzin JA, King KF, Ganin A, Pelc NJ, Glover GH. Concomitant gradient terms in phase contrast MR: analysis and correction. Magn Reson Med 1998;39:300–308.
18. Thunberg P, Wigström L, Ebbers T, Karlsson M. Correction for displacement artifacts in 3D phase contrast imaging. J Magn Reson Imaging 2002;16:591–597.
19. Conturo TE, Smith GD. Signal-to-noise in phase angle reconstruction: dynamic range extension using phase reference offsets. Magn Reson Med 1990;15:420–437.
20. de Zwart JA, Ledden PJ, Kellman P, van Gelderen P, Duyn JH. Design of a SENSE-optimized high-sensitivity MRI receive coil for brain imaging. Magn Reson Med 2002;47:1218–1227.
21. Weiger M, Pruessmann KP, Leussler C, Röschmann P, Boesiger P. Specific coil design for SENSE: a six-element cardiac array. Magn Reson Med 2001;45:495–504.
22. Ohliger M, Ledden P, Yeh EN, McKenzie CA, Sodickson DK. The effect of inductive coupling on parallel image reconstruction. In: Proceedings of the 10th Annual Meeting of ISMRM, Honolulu, 2002. p 197.
23. Preussmann KP, Weiger M, Wiesinger F, Boesiger P. An investigation into the role of coil coupling in parallel imaging. In: Proceedings of the 10th Annual Meeting of ISMRM, Honolulu, 2002. p 196.
24. Weiger M, Pruessmann KP, Boesiger P. 2D SENSE for faster 3D MRI. MAGMA 2002;14:10–19.